University of Huddersfield

University of Huddersfield Repository

Tian, Xiange, Feng, Guojin, Chen, Zhi, Albraik, Abdulrahman, Gu, Fengshou and Ball, Andrew

The investigation of motor current signals from a centrifugal pump for fault diagnosis

Original Citation

Tian, Xiange, Feng, Guojin, Chen, Zhi, Albraik, Abdulrahman, Gu, Fengshou and Ball, Andrew (2014) The investigation of motor current signals from a centrifugal pump for fault diagnosis. In: Comadem 2014, 16th - 18th September 2014, Brisbane, Australia.

This version is available at http://eprints.hud.ac.uk/21737/

COMADEM 2014

16 – 18 September 2014 | Brisbane Convention and Exhibition Centre, Australia

27th International Congress of Condition Monitoring and Diagnostic Engineering

The investigation of motor current signals from a centrifugal pump for fault diagnosis

Xiange Tian[a], Guojin Feng[a], Zhi Chen[b], Abdulrahman Albraik[a], Fengshou Gu[a,b]∗ and Andrew D. Ball[a]

aCentre for Efficiency and Performance Engineering, University of Huddersfield, Queensgate, Huddersfield, HD1 3DH, UK
bSchool of Mechanical Engineering, Taiyuan University of Technology, Shanxi, China, 030024.

PAPER TEXT

In this paper, motor current signals from electrical control systems, rather than installing additional measurement systems, are characterised for the fault diagnosis of centrifugal pumps. Modulation signal bispectrum (MSB) analysis is applied to reveal the weak nonlinear characteristics of current signals when the pump with different impeller faults operates under a wide range of flow conditions. Experimental results show that two static features including the amplitude at supply frequency and the frequency value of bar-passing frequency can be based on to diagnose impeller defects on exit vane tips and inlet vane tips. In addition, the dynamic parameter of sidebands at vane-passing frequency can also be a good indicator for differentiating between the faults.

Keywords: Centrifugal pump; Motor current signature analysis; Modulation signal bispectrum

∗ Corresponding author: Tel.: +44 (0)1484-473548; fax: +44 (0) 1484 473075; e-mail: f.gu@hud.ac.uk

1. Introduction

Centrifugal pumps are widely used in multiple industrial sectors such as petrochemical, water treatment, power generation, agriculture, fertilizers oil and gas, etc.[1]. Most of them are driven by induction motors, and failure to either the motor or the centrifugal pump would result in an unscheduled shutdown leading to loss of production and subsequently loss of revenue. To monitor the condition of motor-pump systems, a great deal effort has been invested in detecting and diagnosing incipient faults in induction motors and centrifugal pumps through the analysis of vibration, acoustic sound, acoustic emission, pressure, flow rate and temperature[2]. However, all of the above mentioned methods require additional sensors to be installed on the system, which leads to an increase in overall system cost. Furthermore, in many cases e.g. submersible pumps it may be difficult to access the pump to install such sensors[3].

Previous studies have shown that motor current signature analysis (MCSA) can be used for condition monitoring of different types of machines, especially, where the use of external sensors are difficult due to insufficient spaces and unusual environmental conditions. Motor current and power analysis methods have been developed to assist in the condition monitoring of a variety of motor-driven devices. In 1988, Kliman et al.[4] proposed that rotor current is sensitivity to detect a single broken bar (and possibly a cracked bar). Casada[5] compared the sensitivity of motor input power and vibration measurements to common sources of vibration and concluded that motor-based measurements are more sensitive to torsionally-related loading than radial or axial vibration data. Casada proposed that the motor can be effectively used as a transducer to aid the understanding of both alignment and process conditions. In contrast, the motor had not been found to be a particularly effective transducer of mechanical unbalance or bearing fault conditions. Casada[6] has also detected a pump specific operational problem by motor current analysis and where the detection of a partial load operation caused by strainer clogging using MCSA was achieved. The motor can be effectively used as a transducer to aid the understanding of both alignment and pump hydraulic conditions. Unsworth J. Peter et al.[7] provided a method for detecting pump cavitation/blockage and seal failure via motor current signature analysis. Welch et al.[8] and Haynes et al.[9] extended the electrical signal analysis to condition monitoring of aircraft fuel pumps. Parasuram P. Harihara and Alexander G. Parlos[10] presented a sensorless approach to detect impeller cracks fault severity in centrifugal pumps. The impeller crack faults are detected using only the line voltages and phase currents of the electric motor driving the pump. The developed fault detection scheme is insensitive to variations in electric power supply and mechanical load. They[11] also proposed a model based method which not only can successfully detect the presence of a bearing fault but also classify bearing degradation in the motor and/or the pump. Fault isolation is carried out using only the line voltages and phase currents of the electric motor driving the pump. The developed fault isolation scheme is insensitive to variations in electric power supply. Augusto and Fredrik[12] performed the diagnosis of a submersible centrifugal pump, proved that it is possible to detect not only when cavitation is present but also when it starts using the current and power signature analyses of its motor drive as diagnostic tools.

Most of the detection schemes presented in the literature mentioned above are based on either tracking the variation of the characteristic fault frequency or computing the change in the energy content of the motor current or in certain specific frequency bands. The characteristic fault frequency depends on the design parameters, which are not easily available. This paper presents a new method of fault diagnosis based on MSB analysis of motor current signals, which has been demonstrated to be particular effect in diagnosing faults from reciprocating compressors[13]. MSB herein is used to capture the deterministic nonlinear feature of modulation components between fluid pulsations, rotating oscillations of the driving shaft and the impeller for reliable diagnosis.

The following content is organized as: Section 2 introduces the theories of motor current based diagnosis. Section 3 descripts the test system. Then, section 4 presents the signal processing results and discussion. Finally, section 5 is the conclusion.

2. Theories of Motor Current based Diagnosis

2.1. Mathematical model of centrifugal pump

To show the feasibility of using motor current data for pump diagnosis, a model for the torque balance of pump system can be developed as Eq. (1)[14].

$$J_m \frac{d\omega}{dt} = T_e - T_l - T_\zeta \qquad (1)$$

where T_e is the active torque produced by the motor; T_l is the passive/load torque created by the pump and mechanical friction losses respectively; T_ζ is the viscous torque; ω is the motor angular velocity; and J_m is the moment of inertia of mechanical system. It shows that any changes of the load torque T_l due to any disturbances such as flow adjustments, external and internal abnormalities would need a corresponding change of the motor torque T_e in order to maintain the speed to be the desired one. Furthermore, the change of the motor torque needs to be compensated by a consistent change of motor current because the motor torque connects to the current as shown in Eq. (2)[15].

$$T_e = \left(\frac{3}{2}\right)\left(\frac{P}{2}\right)L_m(i'_{dr}i_{qs} - i'_{qr}i_{ds}) \qquad (2)$$

where the motor parameters R_s, L_{ls}, R'_r, L'_{lr} and L_m denote the per phase stator resistance, stator leakage inductance, rotor resistance, rotor leakage inductance and magnetizing inductance, respectively. P denotes the number of magnetic poles of the machine. For a given pump system these parameters are fixed. The change in load will not influence them but will alter the current either dynamically or statically depending on the characteristics of load variation caused by flow characteristics.

To understand the load characteristics in the pump system, the model of load torque due to flow effect, which is expressed by Eq. (3)[16], needs to be examined.

$$T_l = a_{t1}Q_i - a_{t2}Q_i^2 + a_{t0}\omega^2 + J_{M_v}\frac{d\omega}{dt} - K_Q\frac{dQ_i}{dt} \qquad (3)$$

where Q_i is the volume flow and its associated coefficients which relates to sizes of the impeller and the hydraulic friction due to liquid between the volute and the impeller. Obviously, the first three terms are the static loads due to steady flow, whereas the other two terms with time differentiation are the dynamic loads due to unstable flow. The dynamic loads are due to the changes in speed and flow which are correlated by parameters of J_{M_v} and K_Q representing the moment of inertia of the water inside the impeller and the effects of flow changes on the impeller torque respectively.

Eq. (3) shows that any abnormalities inside a pump such as defects on impellers due to inventible cavitation and erosions will

cause changes in both static torque and dynamic torque, which in turn influence both the static portion and dynamic portion of the current data. This means that both the static current components and dynamic components will be useful for fault diagnosis.

Moreover, the impellers have limited number of vanes. The flow will be modulated by each vane and exhibit impulsive behavior, which will also be reflected to the current through the dynamic torque terms in Eq. (3). Obviously, the change of vane patterns due to erosions will alter the impulsive behavior. Therefore, detecting these corresponding changes in motor current signals will also allow the monitoring of impeller health conditions.

2.2. MSB analysis

The static portion in current signal is the root mean squared (RMS) value of a measured current signal at supply frequency, which is the dominant component and easy to obtain. However, the dynamic current components need careful handlings in order to calculate from the measured signal because it is very small and can be easily degraded by noise. Based the studies in [13, 17], the current signal i^F including both the static and dynamic components can be expressed as the sidebands at f_F around the dominant components at supply frequency f_s by

$$
\begin{aligned}
i^F = & \sqrt{2} I_s \cos(2\pi f_s t - \alpha_\phi) \\
& + \sqrt{2} I_{Fl} \cos[2\pi (f_s - f_F)t - \alpha_F - \Delta\varphi_{Zl}] \\
& + \sqrt{2} I_{Fr} \cos[2\pi (f_s + f_F)t - 2\alpha_\phi + \alpha_F + \Delta\varphi_{Zr} - \pi]
\end{aligned}
\tag{4}
$$

where I_s, $I_{Fl} = 2\pi(1 - f_F) f_s \Delta\phi/(Z - \Delta Z)$ and $I_{Fr} = 2\pi(1 + f_F) f_s \Delta\phi/(Z + \Delta Z)$ denote the RMS values of current components at supply frequency, lower sideband and high sideband respectively, and the phase terms: α_ϕ, α_F and $\Delta\varphi_Z$ are the initial phase of magnetic flux, fault and change of impedances respectively. It will be shown that an adequate connection between the phase terms in Eq. (4) will make the signal segment independent of different measurement realizations for an effective average process. The average process is critical in extracting the effect of sideband components, because they are small in amplitudes and contaminated with different noises such as that from measurement systems, electrical control systems and disturbances of randomness in fluid flow and mechanical interacts.

As shown in [13, 17] the small sideband in current signal can be better estimated by MSB analysis. The bispectrum, Fourier transform of the third-order cumulant, is a statistic used to suppress Gaussian noise or detect nonlinear interactions. However, conventional bispectrum is not adequate to describe modulation signals like Eq. (4). To overcome this disadvantage, a MSB was proposed in [18, 19]. In this method, the constant phase between the two sidebands of modulated signal is considered in the form of Eq. (5):

$$
B_{MS}(f_1, f_2) = E\left\langle X(f_2 + f_1)X(f_2 - f_1)X^*(f_2)X^*(f_2)\right\rangle
\tag{5}
$$

where $X(f)$ is the Discrete Fourier transform(DFT) of current signal $x(t)$; f_2 is the frequency of carrier signal and f_1 is of modulated signal; $X(f_2)$ is Fourier transform of the carrier and $X^*(f_2)$ is conjugate of $X(f_2)$. The magnitude and phase of MSB can be expressed as Eq. (6) and (7).

$$
A_{MS}(f_1, f_2) = \left| E\left\langle X(f_2 + f_1)X(f_2 - f_1)X^*(f_2)X^*(f_2)\right\rangle \right|
\tag{6}
$$

$$
\phi_{MS}(f_1, f_2) = \phi(f_2 + f_1) + \phi(f_2 - f_1) - |\phi(f_2)| - |\phi(f_2)|
\tag{7}
$$

Based on Eq. (7), the phase combination of Eq. (4) will be

$$
\phi_{MS}(f_1, f_2) = \Delta\varphi_{Zr} - \Delta\varphi_{Zl} - \pi
\tag{8}
$$

It means that the phase of MSB will be constant. The statistical average $E\langle\ \rangle$ of complex value DFT results can be carried out between different signal segments.

Eq. (5) takes into account both $(f_2 - f_1)$ and $(f_2 + f_1)$ simultaneously in Eq. (4) for measuring the nonlinear effects of modulation signals. If $(f_2 - f_1)$ and $(f_2 + f_1)$ are both due to the nonlinear effect between $(f_2 - f_1)$ and $(f_2 + f_1)$, there will be a bispectral peak at bifrequency $B_{MS}(f_1, f_2)$ [13]. On the other hand, if these components are not coupled but have random distribution, the magnitude of MSB will be close to nil. In this way, it allows the wideband noise in signals to be suppressed effectively, so that the phase coupling components can be obtained more accurately.

To measure the degree of coupling between three components, a MSB bicoherence can be used and calculated by Eq. (9)[17].

$$
b_{MS}^2(f_1, f_2) = \frac{\left|B_{MS}(f_1, f_2)\right|^2}{E\left\langle\left|X(f_2)X(f_2)\right|^2\right\rangle E\left\langle\left|X(f_2 - f_1)X(f_2 + f_1)\right|^2\right\rangle}
\tag{9}
$$

3. Test system

Figure 1 shows a photo of the test rig used in this study. With the layout of flow circuitry, the centrifugal pump can deliver 250 l/min of water under a pressure of 10 bar when the driving motor operates at a rated speed of 2900 rpm. As shown in Figure 1, the discharge flow can be adjusted by the discharge control valve to test the pump under different heads and flow rates, allowing its characteristics to be examined over its full operating range.

The experiment was carried out based on a same pump casing but with three different impellers. The first impeller is a healthy one, whereas the second and third have inlet tip defect and exit tip defect, respectively. As illustrated in Figure 2, the fault of inlet defects was induced to the second impeller by removing a small portion of vane tips on the edge close to the inlet. In the same way the exit fault was created on vane edges of the exit side. These faults are typical erosion modes reported in previous studies. To make it clear, the defect positions on impeller are shown as the black areas in Figure 3.
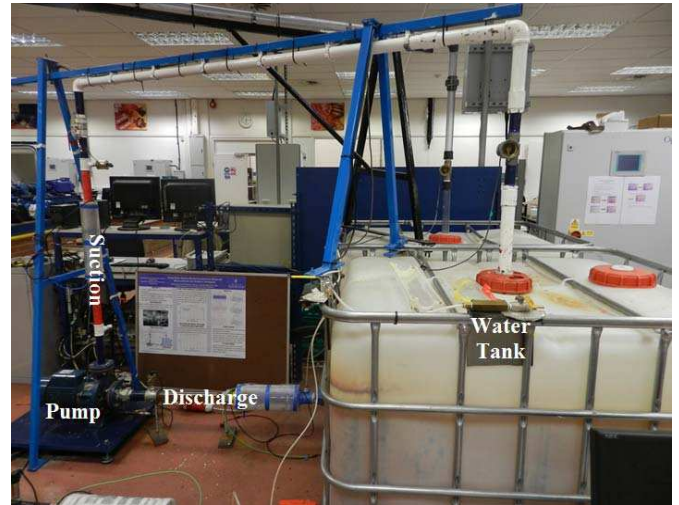

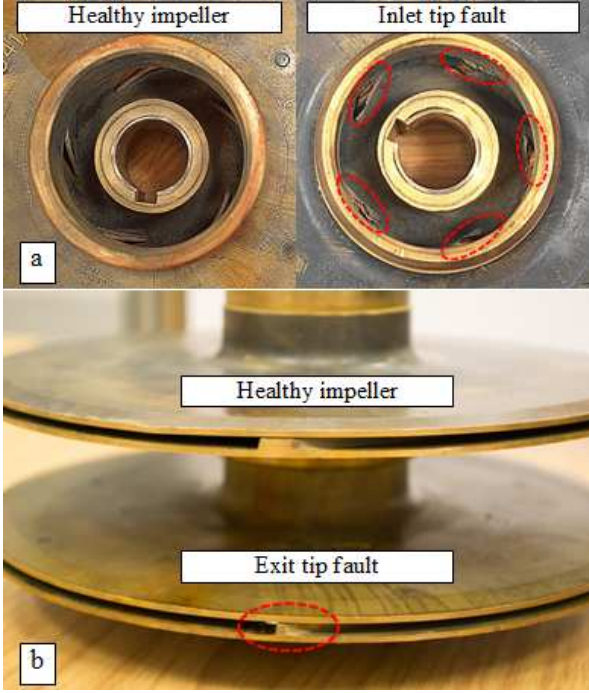**Figure 1** Photo of the pump test rig

Figure 2 Photo of the healthy and faulty impellers

During tests, current signal from motor was collected using a high speed data acquisition system operating at a 96 kHz sampling rate and 24-bit data resolution. Each impeller was installed into the casing in turn and tested at six successive flow rates: 100, 150, 200, 250, 300, and 350 (l/min). In addition, each test was repeated three times for obtaining consistent datasets and reliable comparisons. These multiple test datasets and operating settings will help to understand the current characteristics in Eq. (3) and develop reliable diagnostic features.
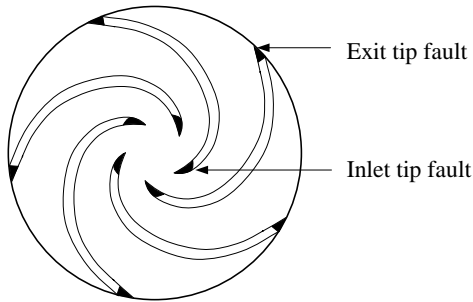

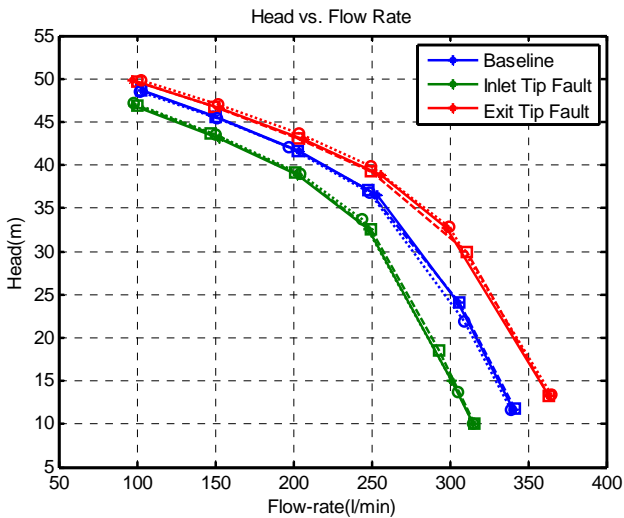**Figure 3** Schematic diagram of impeller defects

Figure 4 The change of pump performance

Figure 4 shows the main performance curves for three cases. It can be seen that the inlet tip fault degrades the performance, which is expected. Surprisingly, the exit tip fault has led to an increase of the performance. It can be understood that the original design may not be optimal and revision of the vane tip may improve the main performance of the pump, though this change may not make the efficiency optimal. Nevertheless, these two faults have changed the optimal operation. It is expected that these changes can be diagnosed from current signals measured from the power supply station which is remote to the pump and motor.

4. Results and discussion

4.1. Characteristics of current signal spectrum

The measured signal was firstly processed by conventional spectrum analysis. From the spectrum shown in Figure 5, it has been found that in addition to the component at $f_s = 50Hz$, the signal contains a string of harmonic components such as at $3f_s$, $5f_s$ and so on, which are due to the electrical supply and motor operation and less correlated with pump operation.

To explore the sidebands of vane-passing frequency, the spectrum is magnified in the low frequency range as shown in Figure 5(b). However, the sidebands and their possible changes with tested cases cannot be undoubtedly observed because of the high level of noise and other components close to $f_{vp} \pm f_s$.

In addition, these sidebands may be suppressed due to the effect of the heavy damping of the fluid which is shown in Eq. (1) as the dynamic viscosity torque. Moreover, the frequency difference between f_{vp} and f_s is large, which will also lead to an additional decreased amplitude due to the effect of impedance change in the motor circuitry as indicated in Eq. (2).

Besides, in the high frequency range, a number of spectral peaks associated with the rotational speed exhibit noticeable changes. As shown Figure 5(c), the sidebands at the bar-passing frequency f_{bp} show distinctive peaks and their frequency values changes significantly with the fault cases. However, these sidebands are arisen from the interaction between stator magnetic fields and rotor fields, which are less correlated with the dynamics of the rotor caused by the flow impulsions. Therefore, the change of the amplitude may not be an effective feature for the impulsion. Nevertheless, because these peaks are very distinctive, they will be based on for the estimation of vane-passing frequency by

$$f_{vp} = f_{bp} / N_{bar} - f_s \qquad (10)$$

when the conventional spectrum is used and

$$f_{vp} = f_{bp} / N_{bar} \qquad (11)$$

when MSB is used. It is obvious that the MSB based results will be more reliable as it does not include the possible error due to the estimation of f_s using conventional spectrum.

On the other hand, the frequency location of the sideband will be sensitive to the static torque and hence the static flow. As the torque increases the frequency will decrease due to the increase in motor slip under high motor loads. Therefore, in addition to the static current I_s in Eq. (4), the value of f_{vp} can also be a useful indicator to show the change of static load due to a defective impeller.
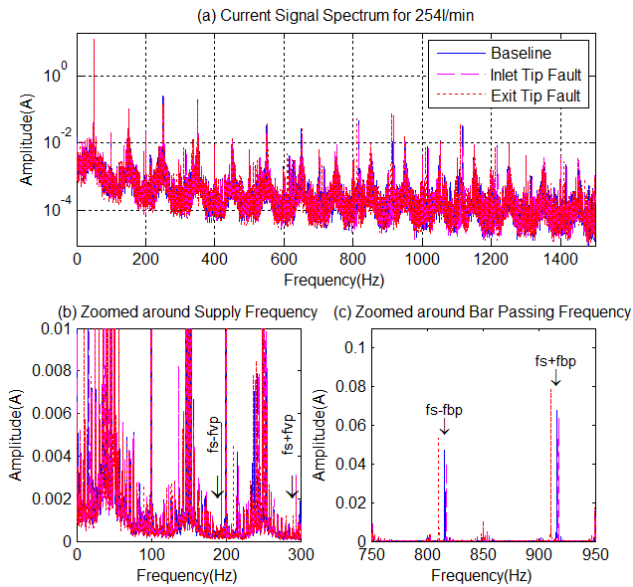
Figure 5 Conventional spectrum of current signal

4.2. Characteristics of current signal MSB

To characterize the sidebands at both f_{vp} and f_{bp}, the MSB expressed in Eq. (4) is applied to current signals to obtain their MSB results in a frequency region specified by frequency ranges of $f_s - 1 \leq f_2 \leq f_s + 1$ Hz and $0 \leq f_1 \leq f_{bp} + 10$ Hz respectively, of which the carrier frequency covers f_2 the possible changes of supply frequency due to instability of the speed controllers. During the calculation, an average of 60 times was achieved based on the length of data records and a Hanning data window was applied to the data segment for suppressing the sidelobes in DFT calculation.
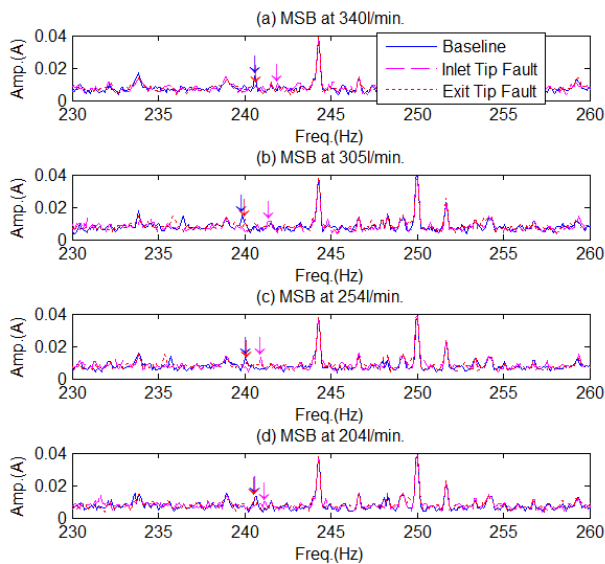

Figure 6 MSB results around f_{vp} at f_s for different flow rates

Fig. 6 shows typical results of the MSB analysis, which is the maximum slice of the carrier frequencies calculated. As shown in the figure, the peaks at f_{vp} are visible and exhibit difference between the tested defect cases. This shows that MSB effectively suppresses the noise in the frequency range of interest. Therefore, it is possible to use this dynamic feature for diagnosing the faults.

4.3. Diagnostic Results

Based on above analysis, three relevant parameters: current amplitude of I_s at f_s, frequency value of f_{vp} and sideband amplitude at f_{vp} are extracted from the MSB results. Figure 7 shows the connection of these parameters to different flow rates. It can be seen that the first two parameters are closely correlated with flow rates. In particular, as the flow increases, the current amplitudes increase correspondingly, showing that more power is required to deliver the high flow. On the other hand, the frequency values exhibit an opposite connection to the flow because of the large slips under high motor loads. As these two parameters are more correlated with the static loads, they are regarded as static parameters.

Moreover, both the current and the frequency values show clear differences from the baseline and between the defective cases. Therefore, it is possible to use either of them to make the difference between the cases for all the low rates, provided the flow parameters can be available.
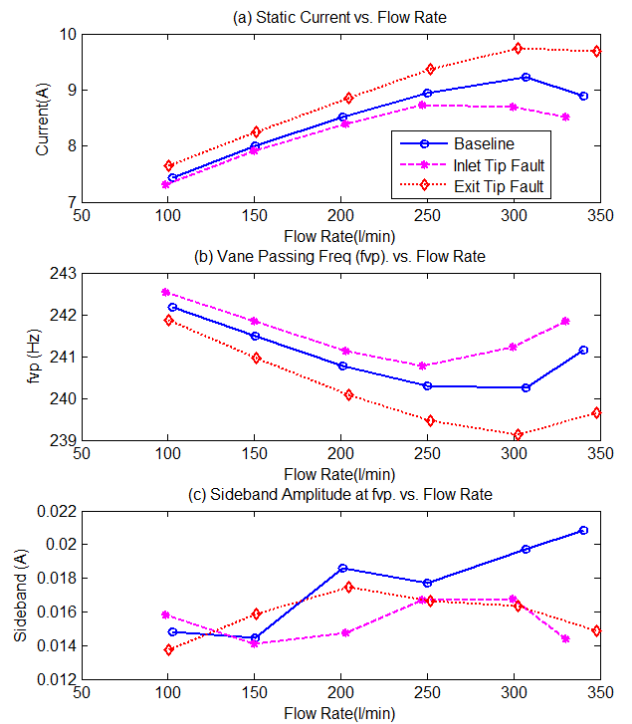

Figure 7 Diagnostic parameters versus flow rate

On the other side, the sideband amplitudes show an increase trend with flow for the baseline case. It indicates that there are more flow pulsations at high flow rates, which agrees with that predicted by the model. However, the defects in both the exit tips and the inlet tips cause a decrease of the sideband. This is also understandable as the defects will reduce the interaction between the flow streams and impeller vanes. Thus, this decrease can be based on to detect the defects but not make difference between them. In addition, the sideband is also unable to make differences for the low flow rates due to the inherent low pulsations induced by the interactions between vane and fluid, which also exhibit further low pulsations under the defective cases and hence difficult to detect.

Obviously, the results are obtained in association with the flow measurements, which is intrusive and difficult to obtain. To show the results based on current measurements only, these three parameters are presented collaboratively as shown in Figure 8. It can be seen in the figure, it is possible to use only current parameters to make differences between the defective cases. For the two static parameters shown in Figure 8(a), a nonlinear classifier such as support vector machine or relevant vector machine may be used to separate the faults from the baseline in

the high flow ranges close to the rated flow condition which are scenarios in which most pumps operation practically. For the combination of static and dynamic based diagnosis as shown in Figure 8(b), a linear threshold can be used to separate the cases in the high flow range.
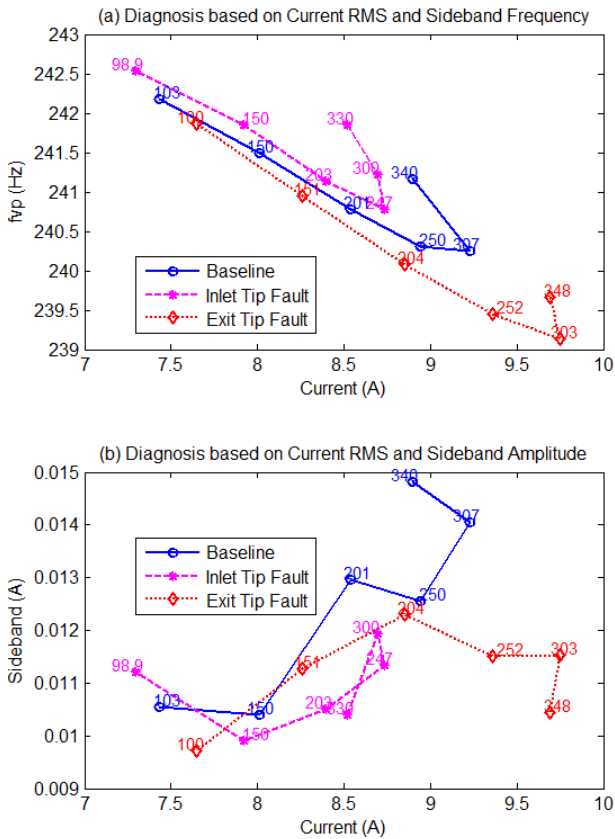

Figure 8 Diagnostic results based on static and dynamic parameters

5. Conclusion

Based on this study it can be concluded that the faults on the impellers of centrifugal pumps can be diagnosed using motor current signals measured remotely. Although the current signal correlates with pump operations in a complicated nonlinear way, it can be examined into static effect and dynamic effect. Both of these effects can be observed in the signals when the impeller is defective. However, the dynamic effect shows very small sidebands at the vane-passing frequency in the spectrum and easily contaminated with noise. Therefore, MSB analysis is applied to extract it. In addition, because of the noise suppression capability, the two dynamic effects: the change of current amplitudes at supply frequency and bar-passing frequency can be estimated more accurately through MSB analysis. Experimental results show that using these three feature parameters, the two types of defective tips on impellers can be diagnosed in the high flow range around the rated flow condition.

References

1. Berli Kamiel, Gareth Forbes, Rodney Entwistle, Ilyas Mazhar and Ian Howard, Impeller Fault Detection for a Centrifugal Pump Using Principal Component Analysis of Time Domain Vibration Features, International Conference Surveillance 7, October 29-30, 2013, Institute of Technology of Chartres, France
2. Parasuram P. Harihara and Alexander G. Parlos, "Centrifugal Pumps", Fault Diagnosis of Centrifugal Pumps Using Motor Electrical Signals, February 24, 2012, ISBN 978-953-51-0051-5.
3. Mohanty, A.R., Pradhan, P.K., Mahalik, N.P. and Dastidar, S.G., 'Fault detection in a centrifugal pump using vibration and motor current signature analysis', Int. J. Automation and Control, 2012, Vol. 6, Nos. 3/4, pp.261–276.
4. Kliman, G.B., Koegl, R.A., Stein, J., Endicot, R.D. and Madden, M.W., 'Non-invasive detection of broken rotor bars in operating induction motors', IEEE Transaction on Energy Conversion, December, 1988, Vol. 3, No. 4, pp.873–879.
5. Casada, D. A. and Bunch, S. L., The Use of Motor as a Transducer to Monitor System Conditions, Proceedings of the 50th Meeting of the Society for Machinery Failure Prevention Technology, pp. 661-672, Jan, 1996.
6. Casada D. A. and Bunch S. L., Integrated Monitoring, Diagnostics and Failure Prevention. Proceedings of a Joint Conference, Mobile, Alabama, April 22-26, 1996.
7. Unsworth, P.J., Discenzo, F.M., Babu, V.S., Detection of pump cavitation/blockage and seal failure via current signature analysis, US 6,757,665 B1, Jun. 29, 2004
8. Welch, D. E., Haynes, H. D., Cox, D. F., & Moses, R. J., Electric Fuel Pump Condition Monitor System Using Electrical Signature Analysis, US Patent No: US 6,941,785, Sept 2005.
9. Haynes, H. D., Cox, D. F. & Welch, D. E., Electrical Signature Analysis (ESA) as a Diagnostic Maintenance Technique for Detecting the High Consequence Fuel Pump Failure Modes, Presented at Oak Ridge National Laboratory, Oct 2002.
10. Harihara, P. P. and Parlos, A. G., Sensorless Detection of Impeller Cracks in Motor Driven Centrifugal Pumps, Proceedings of ASME International Mechanical Engineering Congress and Exposition, pp. 17-23, ISBN 9780791848661, Boston, MA, USA, Oct 31 – Nov 6, 2008.
11. Harihara, P. P. and Parlos, A. G., Sensorless Detection and Isolation of Faults in Motor-Pump Systems, Proceedings of ASME International Mechanical Engineering Congress and Exposition, pp. 43-50, ISBN 9780791848661, Boston, MA, USA, Oct 31 – Nov 6, 2008.
12. Hernandez-Solis, A. and Carlsson, F., Diagnosis of Submersible Centrifugal Pumps: A Motor Current and Power Signature Approaches, EPE Journal, vol. 20, no. 1, (Jan-March, 2010), pp. 58-64, ISSN 0939-8368.
13. Gu, F., Shao, Y., Hu, N., Naid, A., Ball, A. D., Electrical motor current signal analysis using a modified bispectrum for fault diagnosis of downstream mechanical equipment, Mechanical Systems and Signal Processing, 25(1), 360-372, ISSN 0888-3270, 2011.
14. Gordana Janevska, Mathematical Modeling of Pump System, The 2nd Electronic International Interdisciplinary Conference, September, 2-6, 2013.
15. Lipo, T.A., Electric Machine Analysis and Simulation, in: Wiley Encyclopedia of Electrical and Electronics Engineering. John Wiley & Sons, Inc., 2001.
16. Kallesøe, C, Fault Detection and Isolation in Centrifugal Pumps. Ph.D. thesis, Department of Control Engineering, Aalborg University, Aalborg, 2005.
17. Gu, F.; Wang, T.; Alwodai, A.; Tian, X. E.; Ball. D.A. A New Method of Accurate Broken Rotor Bar Diagnosis based on Modulation Signal Bispectrum Analysis of Motor Current Signals, Accepted by MSSP, March 2014.
18. Jouny, I. I., Moses, R. L. Bispectra of modulated stationary signals, IEE Electronics Letters 30(18), 1465–1466, 1994.
19. Stack, J. R., Hartley, R.G., Habetler, T. G., An amplitude modulation detector for fault diagnosis in rolling element bearings, IEEE Transactions on Industrial Electronics, 51(5), 1097–1102, 2004.